Attitude Stability and Altitude Control of a Variable-Geometry Earth-Orbiting Solar Sail

Leonard Felicetti[1,2,3]
Luleå University of Technology, Kiruna, Sweden

Matteo Ceriotti[4] and Patrick Harkness[5]
University of Glasgow, Glasgow, United Kingdom

A variable-geometry solar sail for on-orbit altitude control is investigated. It is shown that, by adjusting the effective area of the sail at favorable times, it is possible to influence the length of the semi-major axis over an extended period of time. This solution can be implemented by adopting a spinning quasi-rhombic pyramidal solar sail which provides the heliostability needed to maintain a passive "sun-pointing" attitude and the freedom to modify the shape of the sail at any time. In particular, this paper investigates the variable-geometry concept through both theoretical and numerical analyses. Stability bounds on the sail design are calculated by means of a first-order analysis, producing conditions on the opening angles of the sail, while gravity gradient torques and solar eclipses are introduced to test the robustness of the concept. The concept targets equatorial orbits above approximately 5,000 km. Numerical results characterize the expected performance, leading to (for example) an increase of 2,200 km per year for a small device at GEO.

Nomenclature

$\mathbf{1}$ = Identity matrix

a = Semi-major axis, km

a_1, a_2, a_4 = Coefficients of the characteristic equation

[1] Researcher, Department of Computer Science, Electrical and Space Engineering, Box 812, Rymdcampus, 981 28 Kiruna, Sweden
[2] Honorary Research Associate, University of Glasgow, School of Engineering, James Watt Building South, Glasgow, G12 8QQ, United Kingdom
[3] Postdoctoral Researcher, Sapienza - Università di Roma, Dipartimento di Ingegneria Astronautica Elettrica ed Energetica, via Salaria 851, 00138 Roma, Italy
[4] Lecturer, School of Engineering, James Watt Building South, Glasgow, G12 8QQ, United Kingdom. Corresponding Author: tel. +44 (0)141 330 6465 e-mail: Matteo.Ceriotti@glasgow.ac.uk
[5] Senior Lecturer, School of Engineering, James Watt Building South, Glasgow, G12 8QQ, United Kingdom

$\mathbf{a}$ = Acceleration vector, m/s^2

b = Quasi-rhombic pyramid base length, m

$\hat{\mathbf{c}}_1, \hat{\mathbf{c}}_2, \hat{\mathbf{c}}_3$ = Axes of the inertial reference frame

c_f = Rotational damping coefficient, N m/rad s

d = Distance to principal axis of inertia, m

e = Eccentricity

f = True anomaly, rad

$f_{control}$ = Angle for orbital control law, rad

$\mathbf{F}$ = Force, N

$\mathbf{G}$ = Gyro Matrix

$\mathbf{h}$ = Orbital angular momentum vector per unit mass, km^2/s

h = Module of the orbital angular momentum per unit mass, km^2/s

i = Inclination, deg

I = Moment of inertia, kg m^2

$\mathbf{I}$ = Inertia matrix, kg m^2

k_1, k_2 = Pitch and yaw inertia ratios

$\mathbf{K}$ = Stiffness matrix

l = Length of booms, m

l_{bus} = Spacecraft bus edge length, cm

m = Mass, kg

$\mathbf{M}$ = Mass matrix

$\hat{\mathbf{n}}$ = Unit vector normal to plane

n_0 = Mean motion, rad/s

P_s = Solar radiation pressure at Earth distance, 4.56×10^{-6} N/m^2

$\mathbf{q}$ = $\begin{bmatrix} \alpha_1 & \alpha_2 \end{bmatrix}^T$

$\mathbf{r}$ = Position vector, m or km

r = Distance from the Earth's center, km

R_E = Radius of the Earth, 6371 km

$\hat{\mathbf{r}}_s$ = Sun direction

$\mathbf{v}$ = Velocity vector, km/s

v = Velocity, km/s

t = Time, hours or days

$\mathbf{T}$ = Torque vector, N m

$\hat{\mathbf{t}}$ = Unit vector tangent to plane

S = Surface of each sail face, m^2

s = Variable in the Laplace's domain, rad/s

z_{CM} = Offset between the center of mass and the center of pressure of the sail, m

$\hat{\mathbf{x}}$, $\hat{\mathbf{y}}$, $\hat{\mathbf{z}}$ = Body axes

α = Apex angle of the sail's surfaces, deg

$\boldsymbol{\alpha}$ = Vector of small angular deviation from the pure spin motion, rad

$\alpha_1, \alpha_2, \alpha_3$ = Small angular deviations from the pure spin motion w.r.t. body axes, rad

β = Precession cone angle, deg

γ = Pointing angle, deg

$\boldsymbol{\Gamma}$ = Sail angular momentum, kg m^2/s

Δ = Nutation angle, deg

ε = Obliquity of equator on the ecliptic, 23.5°

η = Sail reflectivity

θ = Boom flare angle, deg

λ = Longitude of the Sun, deg

μ = Planetary constant of the Earth, 3.986×10^5 km^3/s^2

ρ_{boom} = Boom linear density, kg/m

σ = Areal density, kg/m^2

ψ_x, ψ_x, ψ_x = Euler angles around body axes x, y, z measured w.r.t. nominal Sun-pointing attitude, deg

ω_0 = Nominal spin rate, rad/s

$\boldsymbol{\omega}$ = Angular velocity vector in body axes, rad/s

$\boldsymbol{\omega}_0$ = Nominal angular velocity vector in body axes, rad/s

Superscripts

closed = sail in fully closed configuration

damp = damping

eclipse = sail in eclipse mode configuration

open = sail in fully open configuration

(ECI) = Earth-centered inertial frame

Subscripts

0 = At initial time

A, *B* = Boom A, B

bus = Spacecraft bus

CM = Center of mass

d = Disturbance

f = Damping fluid

gg = Gravity gradient

h = Along the out-of-plane direction

i = i-th face

membrane = Sail membrane

n = Along the normal direction

O = Origin of the body reference frame

s = Sun

t = Along the tangential direction

sail = Sail

x, y, z = Components w.r.t. body axes

Operators

$c_{\square}$ = $\cos(\square)$

$s_{\square}$ = $\sin(\square)$

$\dot{\square}$ = Differentiation with respect to time

$\ddot{\square}$ = Double differentiation with respect to time

$\hat{\square}$ = Unit vector representing a direction

$[\square\times]$ = Skew-symmetric matrix

I. Introduction

SOLAR sails have long been proposed for interplanetary travel [1], using sunlight to accelerate across space. In more recent years opportunities arising from highly non-Keplerian behavior, including applications such as displaced orbits [2] and polar loitering [3], have come to be recognized, and attractive concepts such as orbit raising from low Earth orbit [4] and inclination change [5] have been proposed.

To achieve these objectives, some form of control over the direction and magnitude of the thrust produced by the solar sail has usually been required [6]. It has been suggested that the solar sail can be tilted, using moving masses or propellant, as part of an active attitude and orbit control system [7] and that the thrust vector can be modified by changing the reflectivity of the membrane [9]. However the required attitude control becomes challenging in Earth orbit, where the short orbital periods require rapid slew maneuvers of the sail, and indeed some conventional actuators [8] will likely struggle due to the high moments of inertia associated with typical deployed sails. This issue becomes critical in the nanosatellite regime, where the constraints in power and size significantly affect the capabilities of the attitude control system, and even solutions involving changes to the reflectivity of the sail are

unlikely to be successful [9]. Numerous works have designed optimal steering laws for planetary solar sails: Fekete et al. have used averaging methods to raise a low Earth orbit [27]; Macdonald et al. have studied analytical control laws for individual orbital elements and then applied a blending technique [28][29]; Coverstone et al. maximize the instantaneous energy change to escape from a geosynchronous transfer orbit [30]; Borja proposes to orient the solar panels twice per orbit to deorbit a spacecraft; in all these control laws, the maximum sail turning rate is realistically the limiting factor of their efficiency (or even feasibility). Other concepts, such as the photon thrustor [32] and the ramp sail [33] were also envisaged and studied, in order to re-direct part of the acceleration without steering the entire sail. A less demanding slew rate can be achieved when escaping from highly-inclined or polar orbits, which are however more expensive to reach [34]. Inclination change with solar sails was also investigated, again requiring high turning rates[35][36].

To tackle these problems this paper investigates a variable-geometry solar sail based on the quasi-rhombic pyramid (QRP) [23], where the spacecraft bus lies at the apex and deploys booms along the slant edges, such that reflective membranes may fill the slant faces. The center of solar pressure is therefore more distant from the apex than the center of mass (a distance we term the heliostatic margin), and the spacecraft accordingly exhibits longitudinal heliostatic stability as shown in Fig. 1. If undamped, the motion in response to a disturbance is a quasi-harmonic oscillation about the equilibrium position. Additional stability is provided by an axial spin, which maintains the nominal attitude during eclipse, and we note that disturbances are minimized because operation of the QRP requires (and results) in no net torque being applied about the spacecraft itself. The satellite could be released in a spinning state, or the spin could be initiated, for example, through the heliogyro effect or cold jet thrusters.

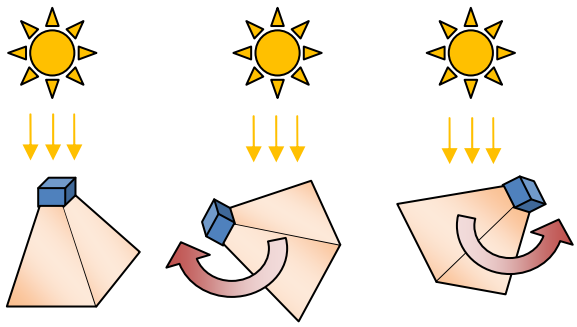

Fig. 1 Heliostability: a restoring moment is produced when the apex points away from the Sun

This paper demonstrates that a QRP-sail can be used to raise or decrease the altitude of a small satellite in a range of circular, equatorial orbits (although this concept is not limited to these). We propose that, above the altitudes associated with major atmospheric perturbations, the solar sail can be opened such that the solar radiation pressure (SRP) provides an accelerating force as the satellite moves away from the Sun, and then closed to minimize the braking force in the second half of the orbit. By operating a QRP-sail in this manner, we will show that the orbit can be raised significantly, especially at higher altitudes (e.g. GEO) where grave-yarding at end-of-life is particularly important. In addition, the control law can easily be reversed to achieve an orbit lowering effect if desired, for example to initiate an orbital transfer that would eventually lead to atmospheric re-entry.

Orbital maneuvers of the type described in this paper could obviously be performed by orienting a flat solar sail alternately normally and as a knife-edge to the sun vector, exactly as described in Ref. [31]. However, the QRP approach offers some distinct advantages. For example, the shape-changing maneuver can be conducted without the need for momentum wheels to execute two slews per orbit, and there are no out-of-plane forces generated during the transition itself. More generally, the overall magnitude of the SRP force generated by the sail can be 'throttled' by adjusting the flare angle without any undesired force components being generated at all, which is something only previously achievable using techniques based on changing the reflectivity of the membrane [37]. The concept is obviously limited by atmospheric drag, but above the upper atmosphere both orbit raising and orbit lowering may be achieved by harnessing the action of sunlight alone.

The paper is organized as follows: Section II is devoted to describing the QRP sail concept, providing the reference frames, the model for the solar radiation acting upon the sail surfaces, the attitude and orbital dynamics, and the orbit control law. Section III addresses the attitude stabilization analytically by applying linearized models and then using the Routh-Hurwitz criterion to obtain useful bounds for the sail design. Finally the numerical results, provided in Section IV, illustrate the expected performance of the sail as well as the robustness of the control strategies against perturbations arising from eclipse, gravity gradient, and the Sun's motion on the ecliptic.

II. The Quasi Rhombic Pyramid Concept

A. Geometry, mass and forces

The QRP spacecraft is composed of a central bus at the apex of a pyramidal sail as depicted in Fig. 2 (a). This paper considers that the booms and membranes have already been deployed, that the structure is rigid, and that any transients have been damped.

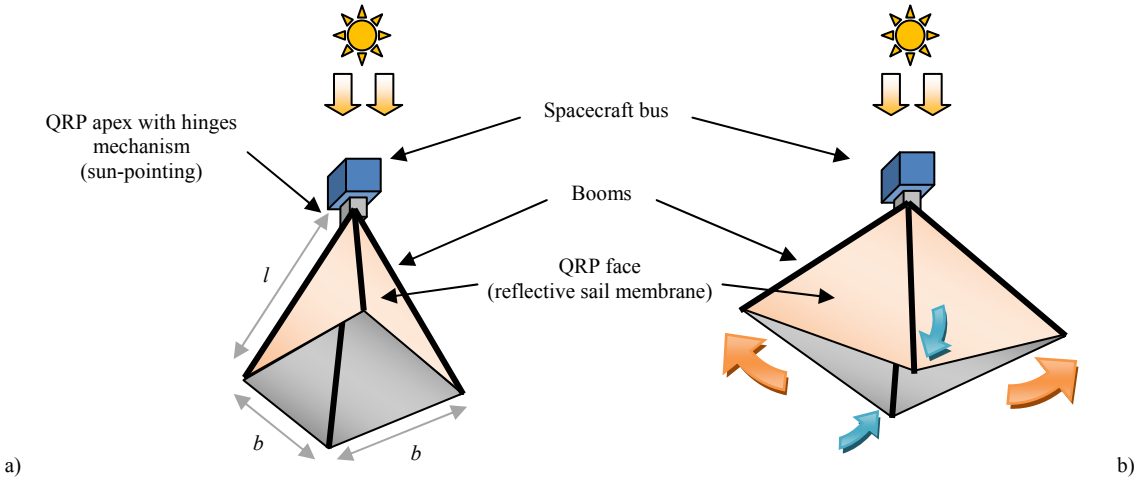

Fig. 2 The quasi-rhombic pyramid concept (QRP).

The size and the shape of each triangular face of the QRP cannot be altered if the membrane is to remain taut, so the four triangular faces are modelled as very thin rigid bodies connected to the booms. The length of base of a triangle is b and the length of the booms is l. Overall three different sail configurations, as the booms move in opposing pairs (θ_A for one pair, θ_B for the opposite pair), are shown in Fig. 3 [23].

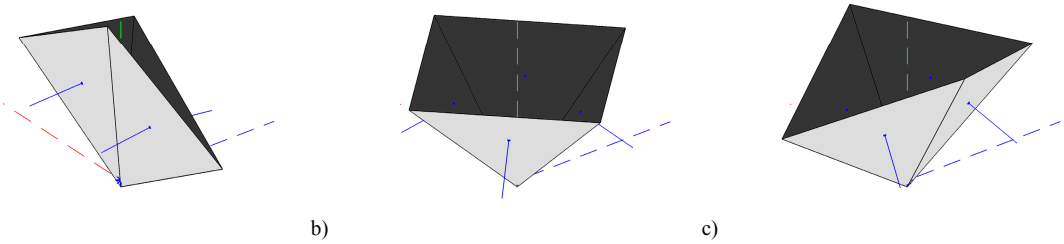

Fig. 3 Sail configurations for $b = l = 1$: a) $\theta_A = 5$ deg; b) $\theta_A = 45$ deg (maximum effective area); c) $\theta_A = 55$ deg. Face normals and principal axes of inertia are also represented.

A uniform areal density σ of the sail material is calculated, taking into account the mass of the booms, while the overall mass of the spacecraft m has two contributions: one due to the sail assembly and one due to the spacecraft bus, which is a uniform cube of side l_{bus}. The centroids of faces of the sail are the points where the solar radiation force, as calculated by integrating the SRP along the surface, is applied. The net force generated by the SRP on each partially reflecting face i, due to specular reflection and absorption, is [21]:

$$\mathbf{F}_i = -(1+\eta) P_s S (\hat{\mathbf{n}}_i \cdot \hat{\mathbf{r}}_s)^2 \hat{\mathbf{n}}_i - (1-\eta) P_s S (\hat{\mathbf{n}}_i \cdot \hat{\mathbf{r}}_s)(\hat{\mathbf{t}}_i \cdot \hat{\mathbf{r}}_s) \hat{\mathbf{t}}_i \tag{1}$$

where $P_s = 4.56 \times 10^{-6}\ \mathrm{N/m^2}$ is the SRP at 1 Astronomical Unit from the Sun, S is the face area, $\hat{\mathbf{n}}_i$ and $\hat{\mathbf{t}}_i$ are the normal and tangential direction respectively, which can be expressed as in Ref. [20], pp. 253. Each face is assumed to have perfectly specular reflectivity and no thermal reemission, but will still have an overall reflectivity efficiency η less than unity due to absorption. The main effect of absorption is to reduce the acceleration magnitude and to introduce a force component tangential to the surface [19] as pointed by $\hat{\mathbf{t}}_i$. In Eq. (1), the direction $\hat{\mathbf{r}}_s$ can easily be calculated, in an Earth Centered Inertial reference frame (ECI) as function of time, by means of [13]:

$$\hat{\mathbf{r}}_s^{(ECI)} = \begin{bmatrix} \cos\lambda & \sin\lambda\cos\varepsilon & \sin\lambda\sin\varepsilon \end{bmatrix}^T, \quad \lambda = \lambda_0 + t\dot{\lambda} \tag{2}$$

where λ is the longitude of the Sun, $\dot{\lambda} = 1.99 \cdot 10^{-7}\, rad/s$ is the angular velocity of the Earth-Sun system (assumed constant), and $\varepsilon = 23.5\,\mathrm{deg}$ is the obliquity of the equator on the ecliptic plane. By choosing $\lambda_0 = 0$, then at time $t = 0$ the Sun is at the vernal equinox in the equatorial plane (Fig. 4).

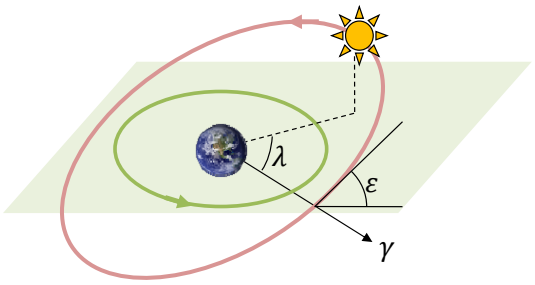

Fig. 4 Apparent orbit of the Sun as seen from an Earth-centered inertial reference frame.

The force $\mathbf{F}_i$ is only experienced on a face lit by the Sun, i.e. $\hat{\mathbf{n}}_i \cdot \hat{\mathbf{r}}_s > 0$. As it is considered that the sun is always on the apex side of the device partial illumination of faces does not occur and the total acceleration

experienced by the sail $\mathbf{a}_{sail}$ is simply the sum of the contributions of all the four faces. Torque about the center of mass $\mathbf{T}_{sail}$ may similarly be calculated.

A. Attitude dynamics

The attitude of the QRP sail is described with a rigid body model and the changes in boom configuration are assumed to be instantaneous. The equation of motion for the angular velocity of the sail can be written as [17]:

$$\mathbf{I}\dot{\boldsymbol{\omega}} = -\boldsymbol{\omega} \times \mathbf{I}\boldsymbol{\omega} + \mathbf{T}_{sail} + \mathbf{T}_d \tag{3}$$

The SRP torque $\mathbf{T}_{sail}$ is computed with the correct value of the inertial matrix $\mathbf{I}$ being used according to the flare angle of the booms and the current configuration of the sail. $\mathbf{T}_d$ contains any disturbance torques such as nutation damping and gravity gradient, which is itself modelled as (Ref. [17], pp.188-191):

$$\mathbf{T}_{d,gg} = \frac{3\mu}{r^5}\mathbf{r} \times \mathbf{I}\mathbf{r} \tag{4}$$

where μ is the planetary constant ($\mu = 3.986 \times 10^5$ km^3/s^2). Attitude parameterization is performed by using quaternions (Ref. [17], pp.103-104) to obtain the direction of the Sun $\hat{\mathbf{r}}_s$ in body axes, as required in Eq. (1). Expressions of the damping torque will be provided in Section III.

B. Orbital dynamics

For the purposes of orbital propagation, the Earth's gravity, secular effects due to the Earth's oblateness, and the effect of SRP are considered. Aerodynamic effects are neglected because the lowest orbits in this study are above 1000 km.

The differential equation of motion of the spacecraft, neglecting the Earth's oblateness for the moment, is:

$$\ddot{\mathbf{r}}^{(ECI)} = -\frac{\mu}{r^2}\hat{\mathbf{r}}^{(ECI)} + \mathbf{a}_{sail}^{(ECI)} \tag{5}$$

where $\mathbf{r}$ is the position vector and $\mathbf{a}_{sail}^{(ECI)}$ the acceleration due to the solar radiation both expressed in ECI reference frame.

Due to the magnitude of the perturbing accelerations with respect to the gravitational acceleration, all the Keplerian elements of the orbit except from the true anomaly, f, change very slowly and so the integration is performed using Gauss' variational equations (Ref. [14], pp. 488-489). The secular effect due to Earth's oblateness, or J_2, is

then considered, in terms of regression of the nodes and advance of perigee, where the secular rates can be described as function of semimajor axis, inclination and eccentricity of the orbit (Ref. [17], pp.581-583). Finally, eclipses are modelled without a penumbra, and the spacecraft is considered to be in eclipse when it is inside the ideal cylinder of shadow cast by the Earth. When the spacecraft is in an eclipse condition, $\mathbf{F}_l = 0$, no SRP force and torque are experienced, and therefore the equations of motion are integrated with $\mathbf{a}_{sail} = 0$ and $\mathbf{T}_{sail} = 0$

C. Control Law

This mission concept is intended to allow either an increase or a decrease in the semi-major axis by opening or closing the sail booms in order to control the thrust provided by the SRP. Specifically, by inspecting Gauss' variational equations (Ref. [14], pp. 488-489) it can be seen that, to maximize the semi-major axis change, any acceleration should be tangential to the orbit. Therefore, to increase the semi-major axis, the sail (in its nominal sun-pointing attitude) should be open when the spacecraft is travelling away from the Sun, i.e. $\hat{\mathbf{r}}_s \cdot \hat{\mathbf{v}} < 0$ ($\mathbf{v}$ being the spacecraft velocity) and it should be as closed as possible when the spacecraft is travelling towards the Sun, i.e. $\hat{\mathbf{r}}_s \cdot \hat{\mathbf{v}} > 0$. In this work, equatorial orbits are considered (i.e. zero inclination), for reasons which will become clear later on.

When the sun is in the same plane as the orbit there will only be only one true anomaly in which $\hat{\mathbf{r}}_s, \hat{\mathbf{v}}$ are antiparallel, and thus the only SRP acceleration component is tangential. At all other points the SRP acceleration will have a normal component, and when the Sun is out of the orbital (equatorial) plane, then the SRP acceleration will have an out-of-plane component as well. Therefore, it is decided to open the sail (maximum SRP harnessed) when the spacecraft crosses anomaly $\pi/2 - f_{control}$ (measured starting from Sun direction), and close it (minimum SRP harnessed) when the spacecraft crosses $\pi/2 + f_{control}$. This is equivalent to the following condition:

$$\arccos\left(-\hat{\mathbf{r}}_s \cdot \hat{\mathbf{v}}\right) < f_{control} \tag{6}$$

where the angle $f_{control} \in [0, \pi/2]$ is a control law parameter and can be arbitrarily selected by taking into account some constraints like the eclipse conditions. This will result in a control law similar to that proposed in Ref. [15] for deorbit, by varying the effective area exposed to SRP through changing the pitch of the solar panels.

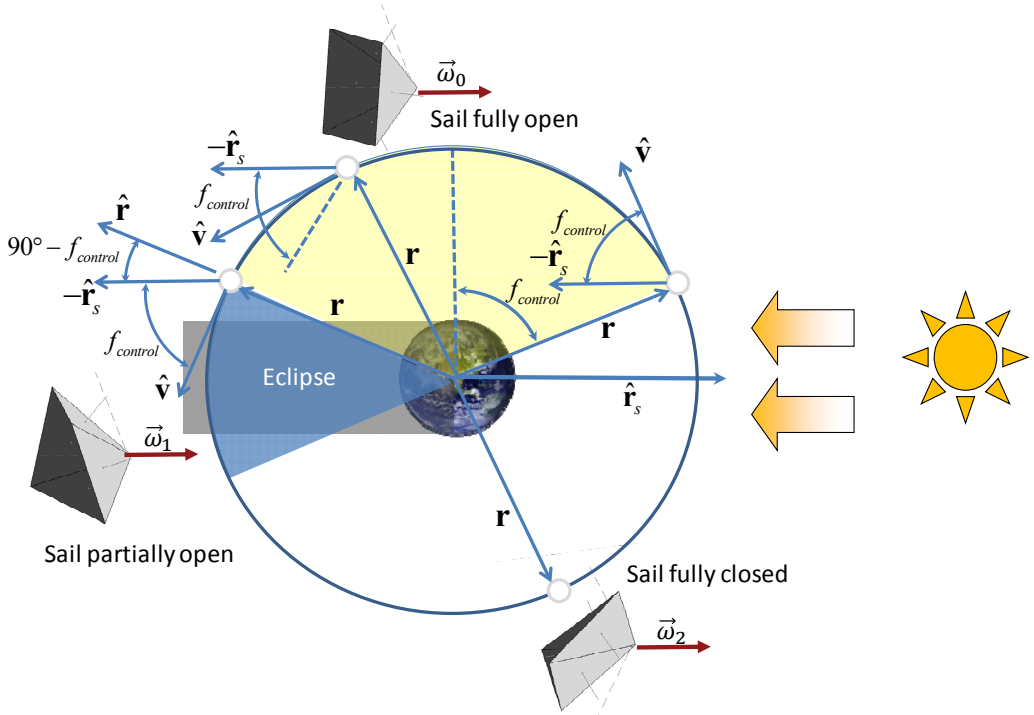

Fig. 5 Orbit control and phases during the orbit

By inspecting the Gauss' variational equation for eccentricity (Ref. [14], pp. 488-489), it is also clear that a tangential acceleration changes the eccentricity of the orbit. The change depends on the true anomaly f, and for a circular orbit ($e = 0$) tends to be positive for one half of the orbit and negative for the other half. This means that the change in eccentricity largely vanishes over the course of a full year due to the Sun's motion about the ecliptic. Similarly, the net change in inclination due to the out-of-plane acceleration component is largely cancelled over a full year due to opposite changes in summer and winter.

Finally, Fig. 5 shows that there is one more phase to take into account: the eclipse. In this region heliostability is lost and small perturbations such as gravity gradient, or even residual angular velocities, can build up to large attitude deviations from the sun-pointing direction unless the sail is reconfigured in order to reduce the unwanted drift. The change of the sail configuration should be performed before the spacecraft enters into the eclipse in order to exploit the remaining heliostability to settle the sail after the shape-changing maneuver, as soon as the following condition is satisfied:

$$\arccos\left(-\hat{\mathbf{r}}_s \cdot \hat{\mathbf{r}}\right) < \frac{\pi}{2} - f_{control} \tag{7}$$

In conclusion, three different sail configurations are used along the orbit:

- Sail *fully open*, when the spacecraft is travelling away from the sun, to maximize the increase in semimajor axis;
- Sail *partially open*, during the eclipse phase, to minimize the impact of perturbations on the attitude, in absence of SRP;
- Sail *fully closed*, when the spacecraft is travelling towards the sun, to minimize the acceleration, which would mainly be against the velocity vector.

III. Attitude Stabilization and Control

The spacecraft nominal attitude is sun-pointing, and to counteract losses of stability associated with the eclipses, the spacecraft is spun around the $\hat{\mathbf{z}}$ body axis. The attitude stability properties in both the illuminated and eclipse phases can be analyzed by linearizing the equations around the nominal configuration of the sail, and considering small displacements of the spin axis with respect to the sun direction, as represented in Fig. 6.

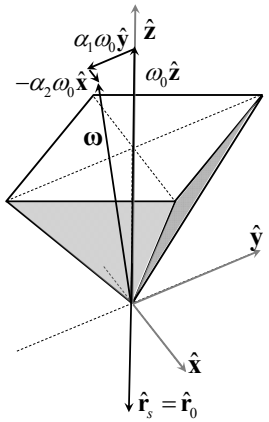

Fig. 6 Small angular deviation with respect to the nominal spin motion

Specifically, let us suppose that the spacecraft is spinning around its principal axis $\hat{\mathbf{z}}$ with a nominal angular velocity $\boldsymbol{\omega}_0 = \omega_0\hat{\mathbf{z}}$. Let us also consider small angular deviations from the pure spin motion $\boldsymbol{\alpha} = [\alpha_1 \quad \alpha_2 \quad \alpha_3]$ with respect to the three body axes respectively, and the corresponding small changes in angular velocity $\dot{\boldsymbol{\alpha}} = [\dot{\alpha}_1 \quad \dot{\alpha}_2 \quad \dot{\alpha}_3]$. The resulting angular velocity can be expressed as follows:

$$\boldsymbol{\omega} = \left(\mathbf{1} - [\boldsymbol{\alpha}\times]\right)\boldsymbol{\omega}_0 + \dot{\boldsymbol{\alpha}} = \begin{bmatrix} -\alpha_2\omega_0 + \dot{\alpha}_1 \\ \alpha_1\omega_0 + \dot{\alpha}_2 \\ \omega_0 + \dot{\alpha}_3 \end{bmatrix} \tag{8}$$

where $\mathbf{1}$ is the identity matrix and $[\boldsymbol{\alpha}\times]$ is the skew-symmetric matrix obtained with components of $\boldsymbol{\alpha}$. By substituting Eq. (8) into Eq. (3) and by neglecting the higher-order terms, one can obtain the following linearized equation of motion about the nominal spin motion for yaw and pitch in matrix form (roll is completely decoupled) (Ref.[20], pp.116-121):

$$\mathbf{M}\ddot{\mathbf{q}} + \mathbf{G}\dot{\mathbf{q}} + \mathbf{K}\mathbf{q} = \mathbf{T} \tag{9}$$

where

$$\mathbf{q} = \begin{bmatrix} \alpha_1 \\ \alpha_2 \end{bmatrix}; \quad \mathbf{M} = \begin{bmatrix} I_x & 0 \\ 0 & I_y \end{bmatrix}; \quad \mathbf{G} = \omega_0 \left(I_x + I_y - I_z \right) \begin{bmatrix} 0 & -1 \\ +1 & 0 \end{bmatrix}; \quad \mathbf{K} = \omega_0^2 \begin{bmatrix} \left(I_z - I_y \right) & 0 \\ 0 & \left(I_z - I_x \right) \end{bmatrix}; \quad \mathbf{T} = \begin{bmatrix} T_x \\ T_y \end{bmatrix}$$

The stability properties of the system are strictly connected to the characteristic equation of this system. In the following subsections three different stability conditions will be developed and analyzed for the three working conditions of the sail: the torque-free case, the illuminated case, and the eclipse case. In order to analyse the stability properties during these phases, some assumptions have been made and a candidate sail design point will be derived and discussed. To this end a parametric study will be performed, by considering a spacecraft with the fixed geometry and mass characteristics listed in Table 1, but varying the following parameters:

- length of the booms of the sail ($l = 1$ m and $l = 2$ m)
- length of the base of the sail b ($0 \le b \le \sqrt{2}l$)
- flare angle θ_A ($0 \le \theta_A \le \alpha$)

where α is the apex angle of the sail's surfaces.

The values in Table 1 are typical of a nanosatellite (CubeSat) and of technology used for the solar sails [24]. The nominal spin rate ω_0 is referred to a fully-open sail ($\theta_A = \theta_B$) and for the other configurations the angular velocity is computed as follows, using the conservation of angular momentum:

$$\boldsymbol{\omega}_1 = \left(\mathbf{I}_1 \right)^{-1} \left(\mathbf{I}_0 \boldsymbol{\omega}_0 \right) \tag{10}$$

where the subscript 0 refers to the sail-open configuration and 1 to any different configuration. Thus, it is assumed that when the flare angle is changed the update is instantaneous and the angular velocity is modified with respect to Eq. (10).

Table 1 Spacecraft data

Bus mass, m_{bus}, kg	1
Bus size, l_{bus}, cm	10
Boom linear density, ρ_{boom}, g/m	16.3
Sail membrane areal density, $\sigma_{membrane}$, g/m^2	13.2
Sail assembly mass per unit area, σ, kg/m^2	0.050
Sail reflectivity, η	0.85
Nominal spin rate, ω_0, rph	10

A. Homogeneous (torque-free) motion

The stability of the system for an ideal torque-free case (free spinning rigid body) is studied first. The characteristic equation of the system reads as:

$$\det\left[\mathbf{M}s^2 + \mathbf{G}s + \mathbf{K}\right] = 0 \Rightarrow s^4 + a_1 s^2 + a_2 = 0 \tag{11}$$

where $a_1 = \omega_0^2\left(1 + k_1 k_2\right)$, $a_2 = \omega_0^4 k_1 k_2$, $k_1 = \left(I_z - I_y\right)/I_x$ and $k_2 = \left(I_z - I_x\right)/I_y$. Therefore the application of the Routh-Hurwitz criterion leads to the well-known result that spin is stable around the largest or smallest axis of inertia of the spacecraft (Ref.[20)], pp.116-121), which can vary its alignment according to the instantaneous sail configuration.

The results of the parametric study are shown in Fig. 7 for boom length $l = 1$ m and $l = 2$ m respectively. Specifically, these plots show the values of the two inertia ratios k_1 and k_2 as a function of the length of the base b of the sail and of the flare angle θ_A. The stable configurations ($k_1 > 0$, $k_2 > 0$) have been shaded in gray. It is noteworthy that different combinations b and θ_A produce both positive and negative values of the two inertia ratios and the stability conditions can be guaranteed only for a subset of the configuration space: small ranges of opening angles and high value of the lengths of the triangle base. The bottom-right halves of these plots, below the diagonal, have not been filled because they contain unfeasible configurations.

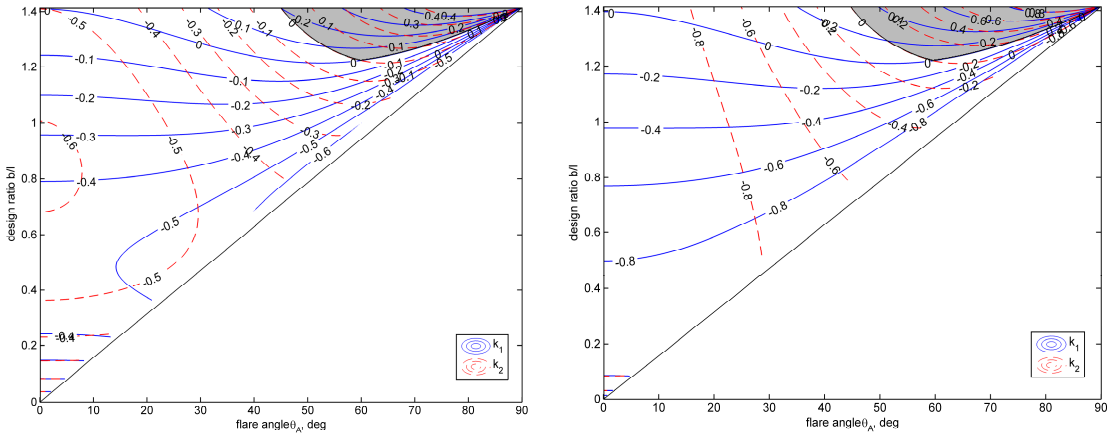

a) b)

Fig. 7 Configuration space with torque-free stable and unstable configurations: (a) l = 1 m; (b) l = 2 m

The stability analysis done so far does not take into account external torques but, during the three phases of the orbital motion the system is forced by the solar radiation torque and the gravity gradient torque. These do change the stability properties of the system as discussed below.

B. Illuminated phase

Due to the particular shape of the sail, the SRP provides a stabilizing torque which increases the stability region for the spin motion of the sail. The stability problem of the pitch-yaw motion of the sail can be analysed starting from Eq. (9), where it is necessary to develop a linearized expression for the solar radiation torque. Equation (1) can be rewritten as follows:

$$\mathbf{F}_i = -2\eta P_s S\left(\hat{\mathbf{n}}_i \cdot \hat{\mathbf{r}}_s\right)^2 \hat{\mathbf{n}}_i - \left(1-\eta\right) P_s S\left(\hat{\mathbf{n}}_i \cdot \hat{\mathbf{r}}_s\right)\hat{\mathbf{r}}_s \tag{12}$$

which can be used for calculating each contribution to the total solar torque due to the each side of the sail as follows:

$$\begin{aligned}\mathbf{T}_{s,i} = \left(\mathbf{r}_{CM,i} - \mathbf{r}_{CM}\right)\times\mathbf{F}_i = -\frac{2}{3}\eta P_s S\left(\hat{\mathbf{n}}_i \cdot \hat{\mathbf{r}}_s\right)^2 \frac{1+c_\alpha}{\sqrt{1-c_\alpha^2}}\left(\mathbf{r}_B - \mathbf{r}_A\right) - \frac{1}{3}\left(1-\eta\right) P_s S\left(\hat{\mathbf{n}}_i \cdot \hat{\mathbf{r}}_s\right)\left(\mathbf{r}_A + \mathbf{r}_B\right)\times\hat{\mathbf{r}}_s \\ +2\eta P_s S\left(\hat{\mathbf{n}}_i \cdot \hat{\mathbf{r}}_s\right)^2 \frac{\left[\left(\mathbf{r}_{CM}\cdot\mathbf{r}_A\right)\mathbf{r}_B - \left(\mathbf{r}_{CM}\cdot\mathbf{r}_B\right)\mathbf{r}_A\right]}{l^2\sqrt{1-c_\alpha^2}} + \left(1-\eta\right) P_s S\left(\hat{\mathbf{n}}_i \cdot \hat{\mathbf{r}}_s\right)\mathbf{r}_{CM}\times\hat{\mathbf{r}}_s\end{aligned} \tag{13}$$

where $c_\alpha = 1 - b^2/(2l^2)$. By assuming that the sail spin axis direction $\hat{\boldsymbol{\omega}}$ is nearly sun pointing, the attitude of the spacecraft can be represented again through a small angular displacement with respect to the nominal direction

through $\boldsymbol{\alpha}$ as defined in Eq. (8). In this case the direction of the nominal motion coincides with the sun direction $\hat{\mathbf{r}}_s$ and therefore, in the body reference frame, the direction $\hat{\mathbf{r}}_s$ can be expressed as:

$$\hat{\mathbf{r}}_s = \left[\mathbf{1} - \left[\boldsymbol{\alpha}\times\right]\right]\hat{\mathbf{r}}_{s,0} \tag{14}$$

where $\hat{\mathbf{r}}_{s,0} = \begin{bmatrix}0 & 0 & -1\end{bmatrix}^T$, as depicted in Fig. 6. Hence, adding up all the contributions of the sides of the sail in Eq. (13), and by considering only the yaw-pitch motion, the total solar radiation torque can be rewritten in a matrix form as follows:

$$\mathbf{T}_{sail} = -\left[\mathbf{K}_{s,1} + \mathbf{K}_{s,2} + \mathbf{K}_{s,3} + \mathbf{K}_{s,4}\right]\begin{bmatrix}\alpha_1 \\ \alpha_2\end{bmatrix} \tag{15}$$

where:

$$\mathbf{K}_{s,1} = \frac{16}{3}\frac{\left(1+c_\alpha\right)\eta P_s S l}{\left(1-c_\alpha^2\right)^{3/2}}\begin{bmatrix} s_{\theta_A}^3 c_{\theta_B} s_{\theta_B} & 0 \\ 0 & s_{\theta_B}^3 c_{\theta_A} s_{\theta_A}\end{bmatrix};\quad \mathbf{K}_{s,2} = \frac{4}{3}\frac{\left(1-\eta\right)P_s S l}{\sqrt{1-c_\alpha^2}}\begin{bmatrix} s_{\theta_A}\left(c_{\theta_A}s_{\theta_B} + 2 s_{\theta_B} c_{\theta_B}\right) & 0 \\ 0 & s_{\theta_B}\left(c_{\theta_B}s_{\theta_A} + 2 s_{\theta_A} c_{\theta_A}\right)\end{bmatrix};$$

$$\mathbf{K}_{s,3} = -16\frac{\eta P_s S z_{CM}}{\left(1-c_\alpha^2\right)^{3/2}}\begin{bmatrix} s_{\theta_A}^3 s_{\theta_B} c_{\theta_B}^2 & 0 \\ 0 & s_{\theta_A} s_{\theta_B}^3 c_{\theta_B}^2\end{bmatrix};\quad \mathbf{K}_{s,4} = -4\frac{\left(1-\eta\right)P_s S z_{CM}}{\sqrt{1-c_\alpha^2}}\begin{bmatrix} s_{\theta_A} s_{\theta_B} & 0 \\ 0 & s_{\theta_A} s_{\theta_B}\end{bmatrix}$$

It is noteworthy that Eq. (15) shows linear relationship between torque and small angles α_1 and α_2, but the coefficient matrix is dependent on the optical properties and on the shape of the sail. Specifically, these matrices are dependent on the two flare angles (θ_A, θ_B) which can be used as control variables. Furthermore, the offset between the center of mass and center of pressure of the sail – the heliostatic margin – also affects the system dynamics.

Inserting Eq. (15) in Eq. (9) leads to the following linearized system:

$$\mathbf{M}\ddot{\mathbf{q}} + \mathbf{G}\dot{\mathbf{q}} + \left[\mathbf{K} + \mathbf{K}_{s,1} + \mathbf{K}_{s,2} + \mathbf{K}_{s,3} + \mathbf{K}_{s,4}\right]\mathbf{q} = 0 \tag{16}$$

Therefore, all the stability properties of the system may be modified by the SRP although we assume that the altitude is sufficient for SRP to dominate gravity gradient and aerodynamic effects. For now this simplifies the analysis by eliminating periodic coefficients but the parametric study, performed by decreasing the orbit altitude, will demonstrate the validity of the underlying hypothesis. Therefore, the new stability conditions can be found through the characteristic equation:

$$\det\left[\mathbf{M}s^2 + \mathbf{G}s + \mathbf{K} + \mathbf{K}_{s,1} + \mathbf{K}_{s,2} + \mathbf{K}_{s,3} + \mathbf{K}_{s,4}\right] = 0 \Rightarrow s^4 + a_2 s^2 + a_4 = 0 \tag{17}$$

and applying again the Routh-Hurwitz criterion. The following system of conditions for stability is found:

$$\begin{cases} a_2 > 0 \\ a_4 > 0 \\ a_2^2 - 4a_4 > 0 \end{cases} \tag{18}$$

These can be used to obtain the indicated flare angles during the illuminated phase, while the parametric study above indicates the configurations which are stable as the SRP is acts upon the sail. The analysis shows that two types of configurations lead to stability. Specifically, when the stiffness matrix given by the sum $\mathbf{K} + \mathbf{K}_{s,1} + \mathbf{K}_{s,2} + \mathbf{K}_{s,3} + \mathbf{K}_{s,4}$ is positive definite the system becomes statically stable, whereas the same matrix is negative definite the system is statically unstable but gyrically stabilized (Ref.[20],pp.121-124). It is worth to note that these two stability cases behave differently when viscous damping is added: the statically stable system becomes asymptotically stable whereas the gyrically stable case becomes unstable. These results are shown in Fig. 8, where the two stable regions are shaded in different gray scales as a function of the base length and the flare angles for the nominal spin rate. These figures provide the upper and lower bounds of the flare angle for a given the pyramid base *b*, which should belong to the statically stable region. Once the sail has been designed (b has been assigned as shown in the dashed lines;), the only in-orbit control parameter for modifying the shape of the sail is the angle θ_A where the admissible range is determined by the intersection of the dashed line with the bounds of the stability region. Specifically, two working configurations can be chosen by means of these plots:

- the *fully-open* configuration maximizes the area exposed to the sun, in order to maximize the SRP thrust. This configuration is achieved when $\theta_A = \theta_B$ leading to [23]:

$$\cos\theta_{A,B} = \sqrt{\frac{2-(b/l)^2}{2}} \tag{19}$$

  and, as a requirement for the sail design, this angle should be within the stable region.

- the *fully-closed* configuration minimizes the area exposed to the solar radiation. This configuration is defined by the lowest value of θ_A inside the stability region (along the ideal, horizontal line representing the selected length *b*).

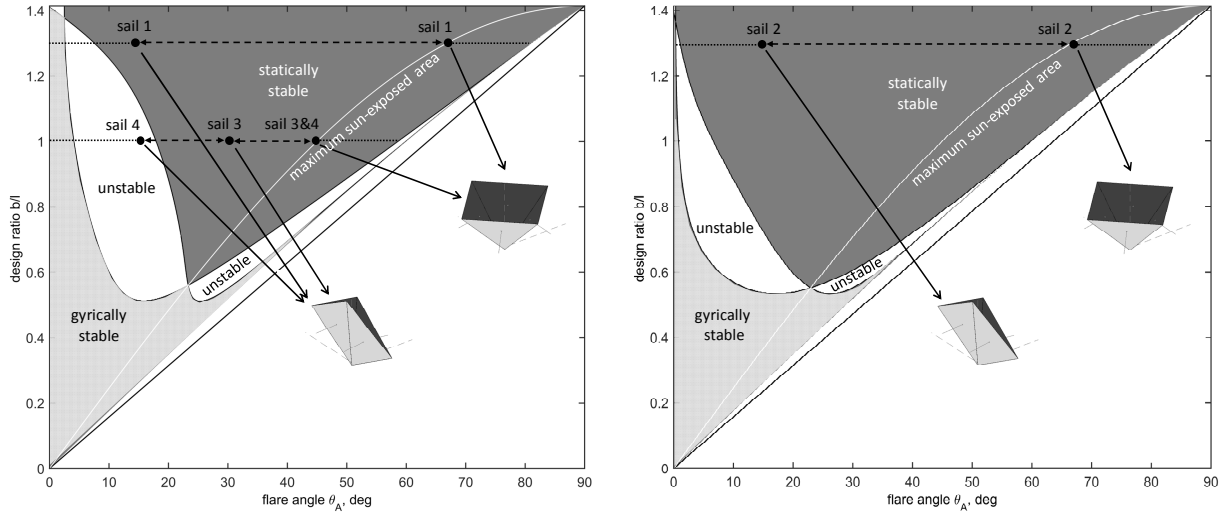

a) b)

Fig. 8 Heliostable configurations. (a) l = 1 m; (b) l = 2 m

C. Eclipse phase

When the spacecraft enters the eclipse, the stabilizing effect of the solar radiation torque disappear and the gravity gradient becomes the dominant forcing term. Therefore only the gyro-stiffness can counteract such perturbations and keep the sail pointing towards an inertially-fixed direction.

Some assumptions are made in order to analyse the stability in this phase. The equations of motion are linearized by assuming that both the sun direction and the spin axis coincide with the local vertical, which is reasonable as eclipse phases happen in the part of the orbit which is opposite to the sun with respect to the Earth. This work assumes that eclipses are short, or equivalently that the orbit is high, which is justified in two ways: a short eclipse means that the low-stability region lasts for a small fraction of the orbital period, while a high orbit means that the gravity gradient is dominated by SRP torque when not in eclipse. Numerical simulations in Section IV, taking into account the full attitude and orbital dynamics, will give quantitative results supporting this statement.

Small angular deviations are introduced in order to represent the local vertical direction in the body reference frame as follows:

$$\hat{\mathbf{r}} = \left[\mathbf{1} - \left[\boldsymbol{\alpha}\times\right]\right]\hat{\mathbf{r}}_0 \tag{20}$$

where $\hat{\mathbf{r}}_0 = \begin{bmatrix} 0 & 0 & -1 \end{bmatrix}^T$, as shown in Fig. 6.

The resulting dynamic system is essentially that in Eq. (9), where the forcing term models the gravity gradient torque. This can be quantified using Eq. (20), linearizing Eq. (4), decoupling the pitch-yaw motion and defining the mean motion as $n_0 = \sqrt{\mu / r^3}$, obtaining:

$$\mathbf{T}_{gg} = 3n_0^2 \begin{bmatrix} (I_z - I_y) & 0 \\ 0 & (I_z - I_x) \end{bmatrix} \begin{bmatrix} \alpha_1 \\ \alpha_2 \end{bmatrix} = -\mathbf{K}_{gg} q \tag{21}$$

leading to a linearized system which reads as:

$$\mathbf{M}\ddot{\mathbf{q}} + \mathbf{G}\dot{\mathbf{q}} + \left[\mathbf{K} + \mathbf{K}_{gg} \right] \mathbf{q} = 0 \tag{22}$$

Once more the characteristic equation is used:

$$\det\left[\mathbf{M}s^2 + \mathbf{G}s + \mathbf{K} + \mathbf{K}_{gg} \right] = 0 \Rightarrow s^4 + a_2 s^2 + a_4 = 0 \tag{23}$$

and the stability is given by the same conditions as in Eq. (18). The set of stable configurations are shaded in Fig. 9 for the two lengths of the sail booms. It can be seen that, in eclipse, for the same length *b*, the stable region is considerably smaller than in illuminated conditions, as expected due to the lack of restoring SRP torque. However, during the eclipse phase, the flare angle θ_A can be adjusted such to preserve stability.

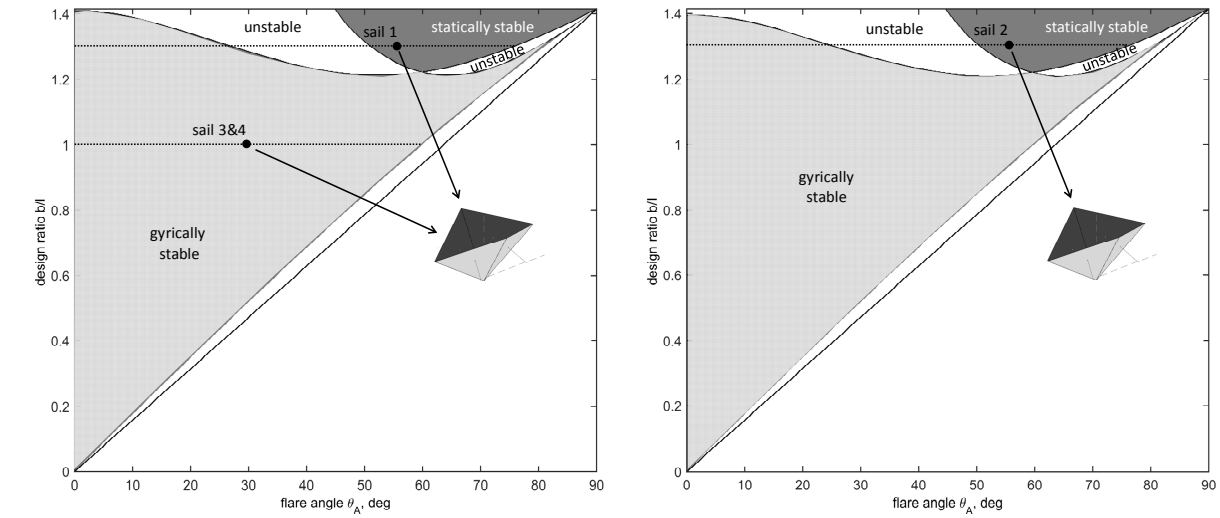

Fig. 9 Stability configurations during the eclipse. (a) *l* = 1 m; (b) *l* = 2 m

IV. Numerical Simulations

The stability analysis performed in Section III showed that, if the sun direction in inertially fixed and the sail is spun about that direction, some stable configurations of base length and flare angles exist. However, the sun direction slowly changes throughout the year, as modelled by Eq. (2), and the linearized analysis does not take into account this variation. In particular, it is necessary to verify that the heliostability guarantees that the sail $\hat{\mathbf{z}}$ axis (spin axis) can follow the sun direction throughout the year. Furthermore, we must recall that the orbit control strategy described in Section II.C requires the sail to reconfigure three times per orbit. Such reconfiguration manoeuvres are fast and may compromise the stability of the system even if such stability is guaranteed in a steady state for the three working configurations of the sail. For this reason, a numerical simulation is performed using the model described above to verify the concept and quantify the change in the semi-major axis. As mentioned previously, all numerical results presented in this section consider eclipses, gravity gradient effects, Earth's oblateness and the Sun's motion along the ecliptic.

The numerical analysis has been performed with four different sails. As set out in Table 2, two different boom lengths are investigated as before ($l = 1$ m and $l = 2$ m), while the lengths of the base of the sail b have been chosen to satisfy both the stability conditions discussed before and mechanical constraints of the boom hinges (reported in Ref. [23]). The limits on the range of the flare angles of the booms are $15 \text{ deg} \le \theta_{A,B} \le 80 \text{ deg}$ and the value of the sail design ratio has been fixed to $b/l = 1.3$ for Sail 1 and Sail 2. This design ratio ensures that the sail can perform the requested open/close manoeuvres while maintaining the flare angles inside the admissible ranges and inside the stability regions. The other two configurations (Sail 3 and Sail 4) of the sail are designed with $l = 1$ m and $b/l = 1$, but different flare angles have been chosen for the mission phases: the fully-closed flare angle of Sails 1, 2 and 3 has been chosen to guarantee their stability, while Sail 4's closed angle has deliberately been chosen to be unstable (see Fig. 8). Finally, the eclipse configurations adopt values so that they might be included in the stable regions of Fig. 9.

Table 2 Sails used for the numerical simulations

		Sail 1	Sail 2	Sail 3	Sail 4*
Boom length, l, m		1	2	1	1
Base of the triangle length, b, m		1.3	2.6	1	1
Flare angle	Fully-closed phase, θ_A^{closed}, deg	15	15	30	15*
	Eclipse phase, $\theta_A^{eclipse}$, deg	55	55	30	30
	Fully-open phase, θ_A^{open}, deg	66.8	66.8	45	45

* Unstable

The case of the spacecraft initially orbiting in a geostationary orbit is considered, with a control anomaly set to $f_{control} = 60\,\text{deg}$, leading to a fully open configuration of 8 hours, an eclipse mode of 3.7 hours and fully closed configuration of 12.3 hours. A representation of the sail during one orbit, including its configurations and attitude, is provided by Fig. 10. The selection of such $f_{control}$ leads to an eclipse starting before and ending after the satellite is in a proper eclipse (which lasts 1.2 hours), in this way it is possible to exploit the heliostabilizing effect of the sun-radiation to counteract the transitions between the operative modes.

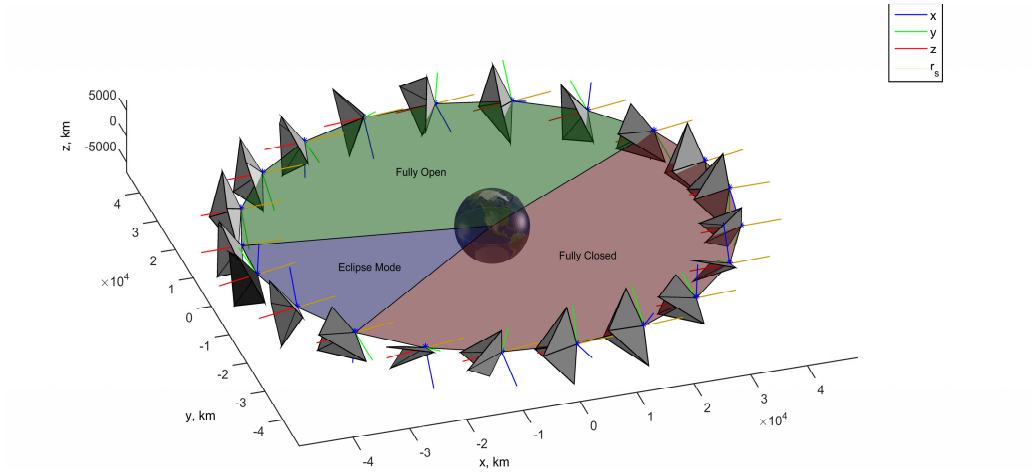

Fig. 10 Representation of the sail during the orbit.

A. Short term behavior

Fig. 11 shows the working mechanism of the variable QRP sail (for the case of Sail 1) during a period of 3 days.

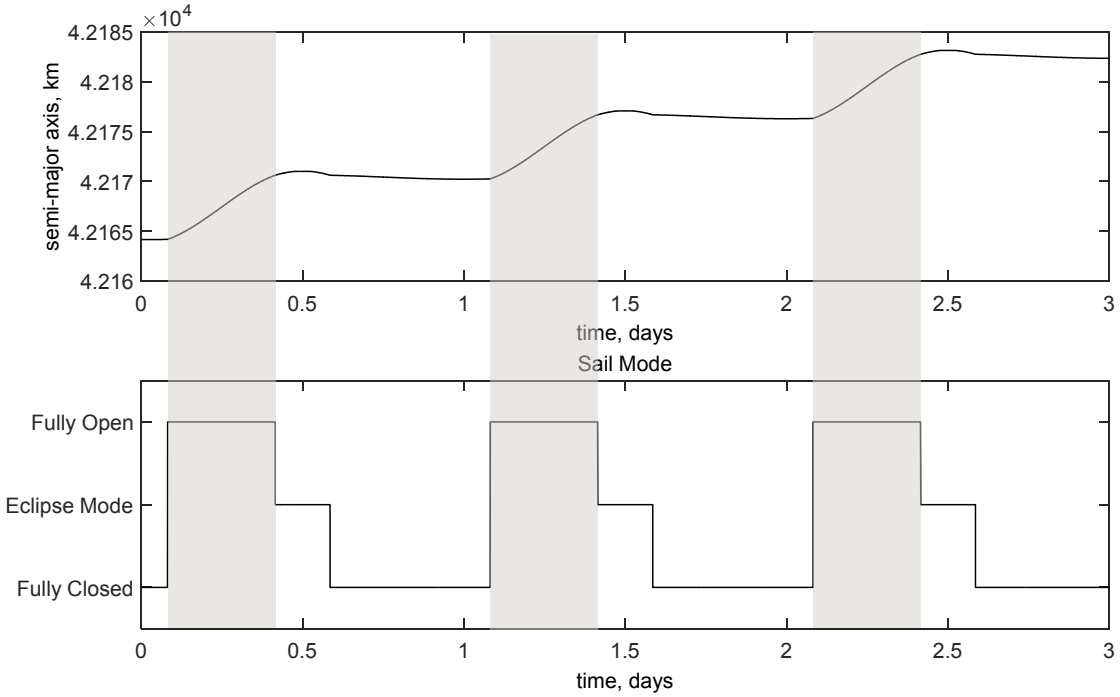

Fig. 11 Orbit raising during the fully opened phases of the sail (Sail 1). Gray bands identify fully-open phases.

Difficulties in attitude stability occur when the sail enters or exits the eclipse. The yaw and the pitch angles with respect to the sun-pointing direction, as well as the two transversal components of the angular velocity, are plotted in Fig. 13. It is apparent that, during the illuminated phase, the attitude of the spacecraft remains almost aligned to the sun-pointing direction, but during the eclipse the stabilizing effect of the solar radiation is not present and the sail-craft starts drifting from the nominal configuration. As a result, when the solar radiation is recovered, the spin axis of the sail is misaligned with respect to the sun and an impulsive torque is applied that causes severe oscillation of the device. This oscillation can lead to instability, as shown for example in Fig. 12.

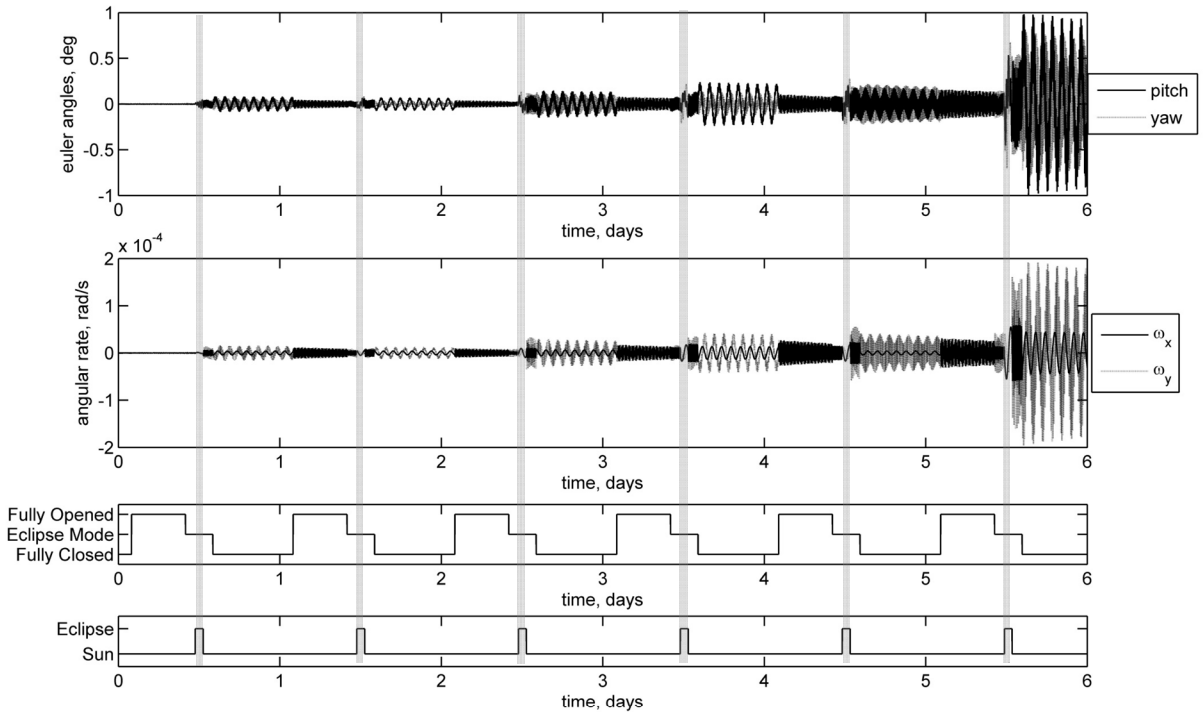

Fig. 12 Attitude with respect to the sun-pointing direction and transversal components of the angular velocity for the undamped case (Sail 1). Gray bands identify eclipses.

1. Damping

In order to reduce the oscillation amplitude, it is proposed to equip the spacecraft with passive nutation dampers along $\hat{\mathbf{x}}$ and $\hat{\mathbf{y}}$ body axes of the sail. These devices usually consist of a sealed ring attached to the spacecraft bus and filled with a viscous fluid. When the spacecraft experiences an angular acceleration, a viscous lag between the bulk fluid and the ring walls dissipates rotational energy as heat [22].

The differential equations of motion of the fluid in each ring may be written by considering that the fluid is accelerated by viscous effects which depend on the relative velocity between the bulk fluid and the ring:

$$\begin{aligned} \dot{\omega}_{f,x} &= -\frac{c_f}{I_{f,x}}\left(\omega_{f,x} - \omega_x\right) \\ \dot{\omega}_{f,y} &= -\frac{c_f}{I_{f,y}}\left(\omega_{f,y} - \omega_y\right) \end{aligned} \tag{24}$$

where $\omega_{f,x}, \omega_{f,y}$ are the angular velocities of the fluid inside the ring and ω_x, ω_y are the two components of the angular velocity of the spacecraft along $\hat{\mathbf{x}}$ and $\hat{\mathbf{y}}$ body axes. In Eq.(24), the coefficient c_f (set $c_f = 1\times10^{-5}$ N m / (rad s) in the simulations) represents the fluid viscosity and I_f is the moment of inertia of the

fluid in the ring. Considering a ring whose radius is half of the spacecraft bus side, and mass 1/20 of the spacecraft bus mass, leads to $I_f = m_{bus}/20 \cdot (l_{bus}/2)^2$.

Therefore, the resulting torque to be applied in Eq. (3) is:

$$\mathbf{T}_d^{damp} = -\begin{bmatrix} I_{f,x}\dot{\omega}_{f,x} - I_{f,y}\omega_{f,y}\omega_z \\ I_{f,y}\dot{\omega}_{f,\mathrm{y}} + I_{f,x}\omega_{f,x}\omega_z \\ I_{f,y}\omega_{f,y}\omega_x - I_{f,x}\omega_{f,x}\omega_y \end{bmatrix} \tag{25}$$

The purpose of the dampers is to reduce the oscillation amplitude during the non-eclipse phases such that, at the next eclipse passage, the sail is almost aligned with respect to the sun.

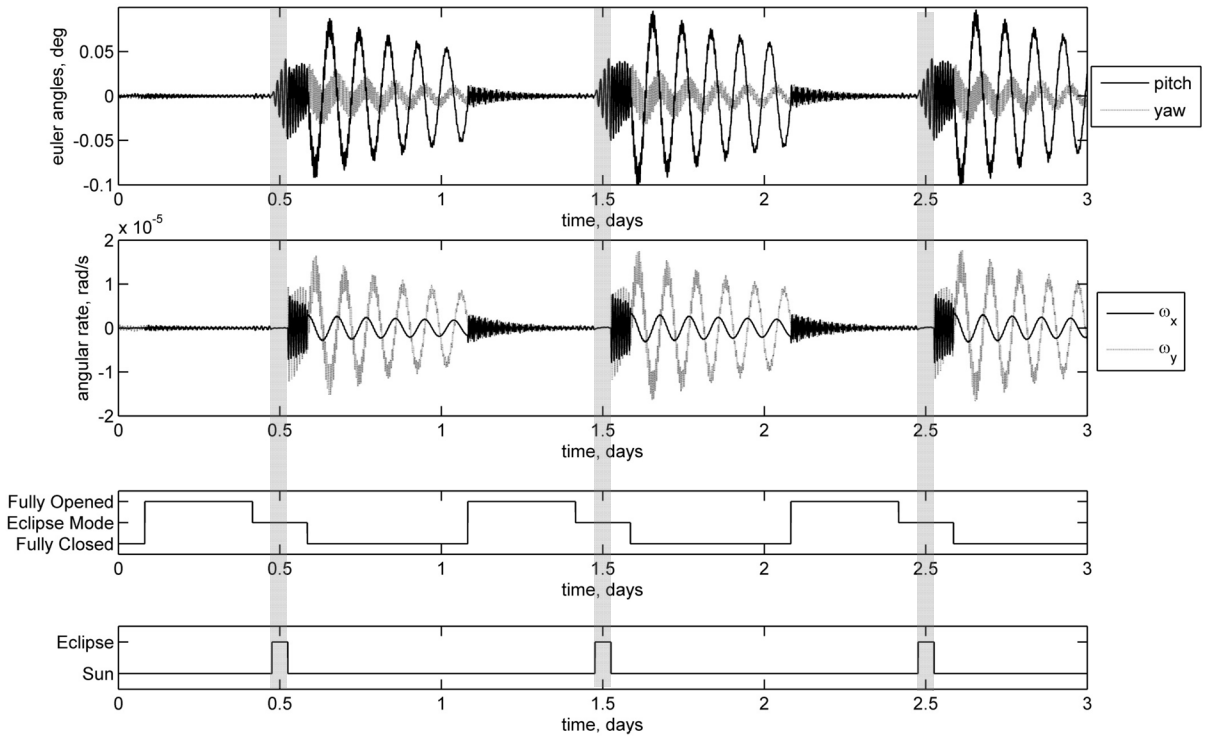

Fig. 13 Pitch and yaw angles with respect to the sun-pointing direction and transversal components of the angular velocity of the Sail 1, with damping. Gray bands identify eclipses.

When the spacecraft reconfigures from the fully-closed to the fully-open configuration a drastic reduction of the transverse components of the angular velocity, as well of the pitch and yaw oscillation amplitude, takes place. This change can be explained analysing the behaviour of the roll angle and of the spin rate along the $\hat{\mathbf{z}}$ axis depicted in Fig. 14. In fact, the spin rate increases significantly when the sail enters its fully-closed configuration, as highlighted

in the gray bands. The increase of the spin rate, due to the changes of moment of inertia, determines a reduction of the transversal components of the angular velocity and therefore reduction of the amplitude of the oscillations perpendicular to the spin direction, as already noticed in Fig. 13.

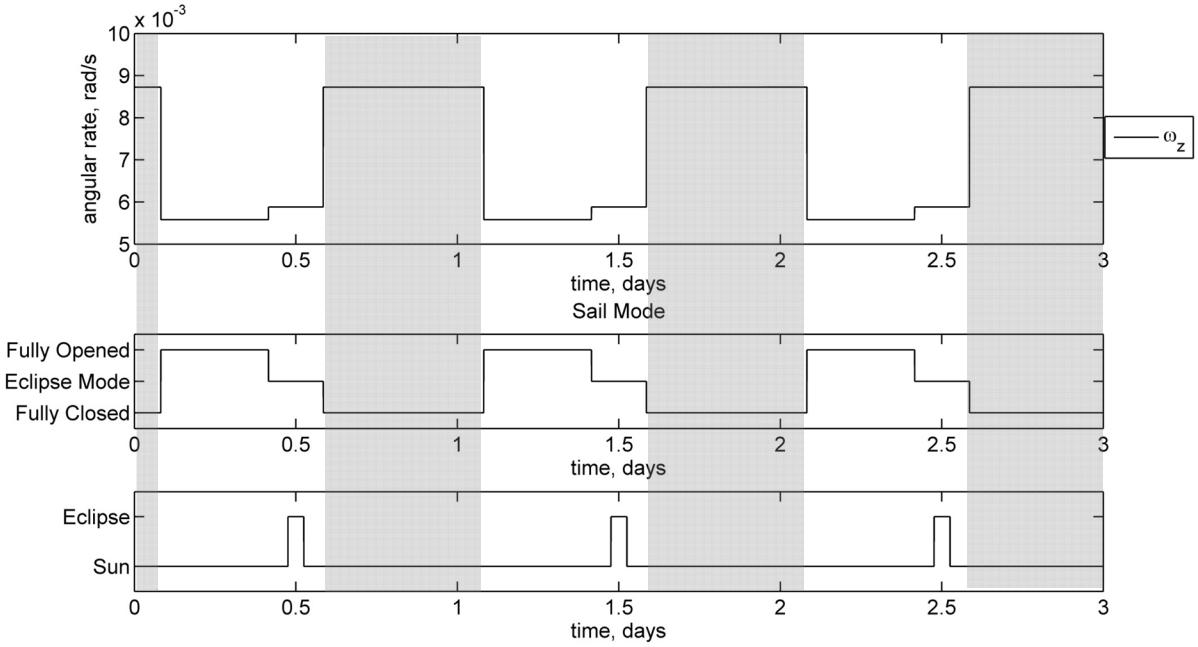

Fig. 14 Spin rate as a function of the sail mode (Sail 1). Gray bands identify the fully-closed phase.

In order to verify the stability bounds found in Section III, a simple test case has been set up by using Sail 4 (unstable): the sail loses its sun-pointing attitude in few orbits, and starts to tumble, as shown by the pitch and yaw angles represented in Fig. 15.

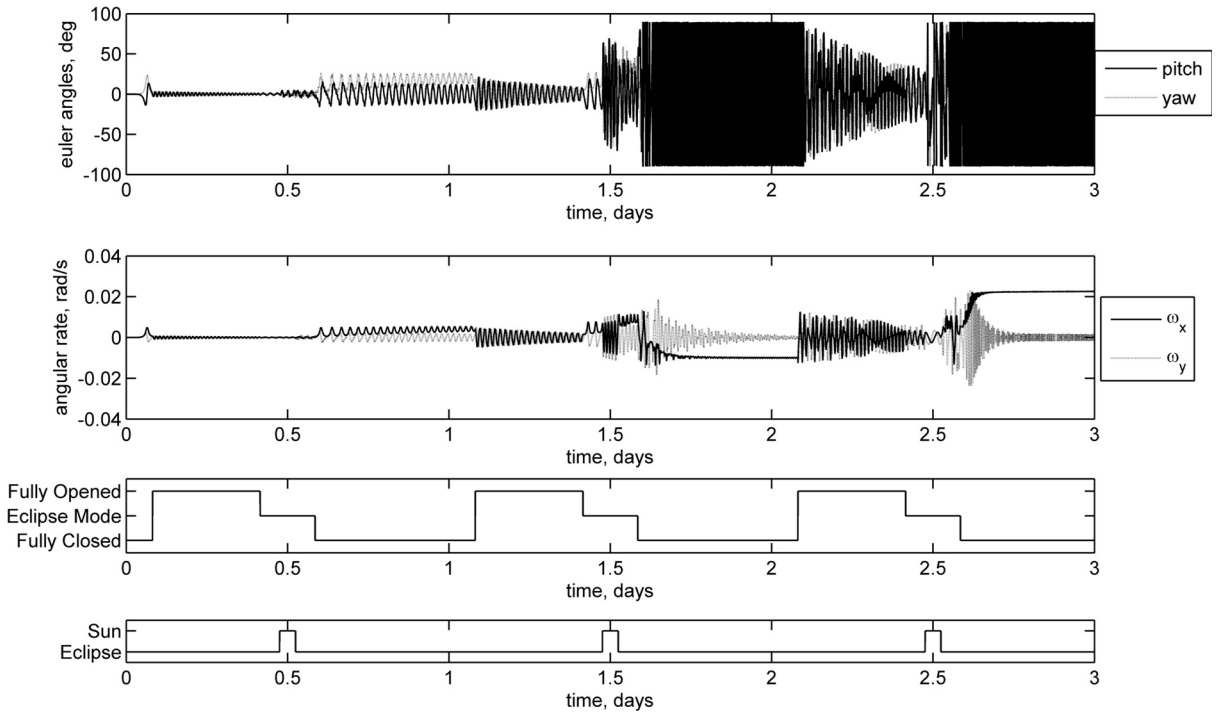

Fig. 15 Unstable attitude behavior of Sail 4

Note that Sail 3 has the same geometry as Sail 4, but it is operated with a different flare angle for the fully-closed configuration and hence it results in a stable behaviour maintaining the sun-pointing condition during all the orbits, as seen in Fig. 16. These results verify numerically the analytical stability study presented in Section III.

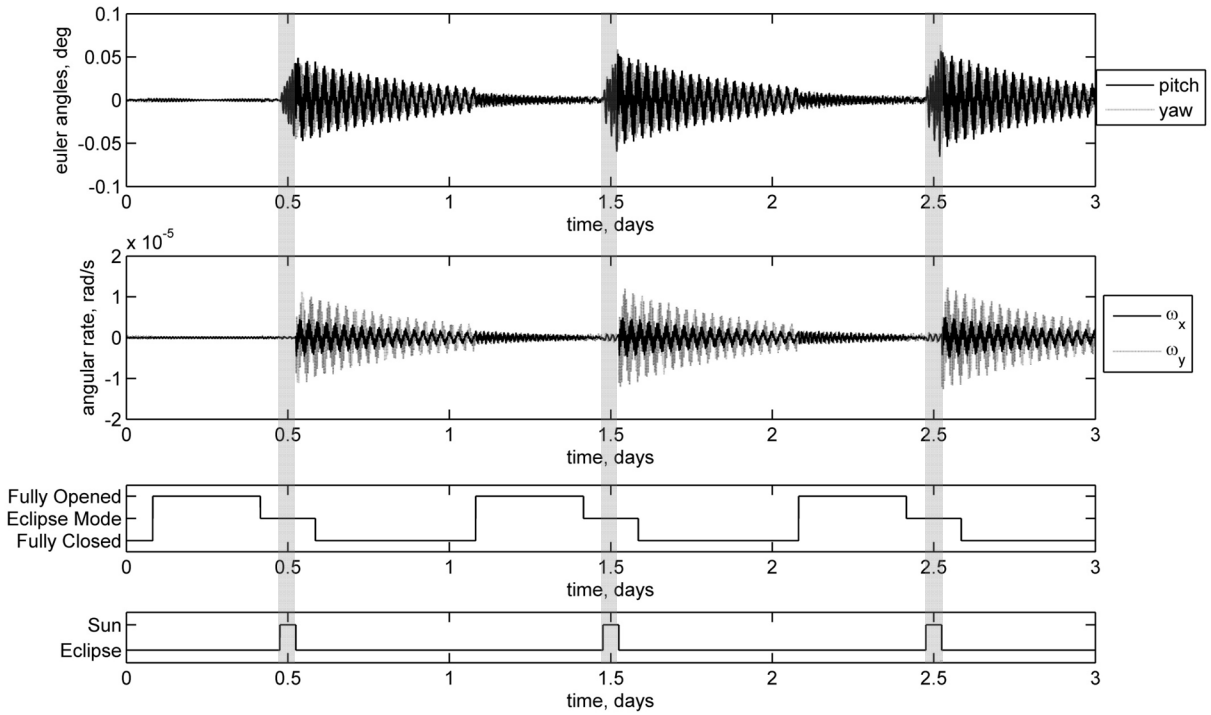

Fig. 16 Stable attitude behavior of Sail 3

B. Short- and long-term sun pointing

Dissipative fluid rings also play a fundamental role in the long-term sun pointing of the sail. As shown in Eq. (2), the sun direction slowly changes throughout the year and the attitude of the sail must follow this change. This is achieved by exploiting both the heliostability of the sail and the dissipative effects of the rings. A qualitative explanation of this process can be obtained by focusing on Fig. 17, where a sketch of the sail attitude motion is represented with respect to an inertial reference frame $\hat{\mathbf{c}}_1\ \hat{\mathbf{c}}_2\ \hat{\mathbf{c}}_3$. Let us assume that initially the $\hat{\mathbf{z}}_0$ axis of the sail, as well as the angular momentum $\hat{\mathbf{\Gamma}}_0$, are perfectly aligned along $-\hat{\mathbf{c}}_3$, as represented by the dotted, light-gray lines in the figure. If the direction of the sun $\hat{\mathbf{r}}_s$ is not perfectly aligned with $\hat{\mathbf{c}}_3$ as represented in figure, a solar radiation torque is applied to the sail $\mathbf{T}_{sr0}$. That torque modifies the direction of the angular momentum to $\hat{\mathbf{\Gamma}}_1$, leading to an increase of the nutation angle Δ_0 (angle between $\hat{\mathbf{z}}_0$ and $\hat{\mathbf{\Gamma}}_1$) and a precession motion of the sail. Therefore the angular momentum of the sail $\hat{\mathbf{\Gamma}}$ describes a cone around the direction $\hat{\mathbf{r}}_s$ and the body of the sail is moved by the drift angular velocity with respect to $\hat{\mathbf{\Gamma}}$ [20]. In general, the $\hat{\mathbf{z}}$ axis of the sail will be misaligned with respect the

actual angular momentum $\hat{\mathbf{\Gamma}}$ of the sail of a nutation angle Δ and the dissipative effects of the damping rings becomes mandatory to reduce Δ and to realign the $\hat{\mathbf{\Gamma}}$ axis towards the $\hat{\mathbf{r}}_s$ direction.

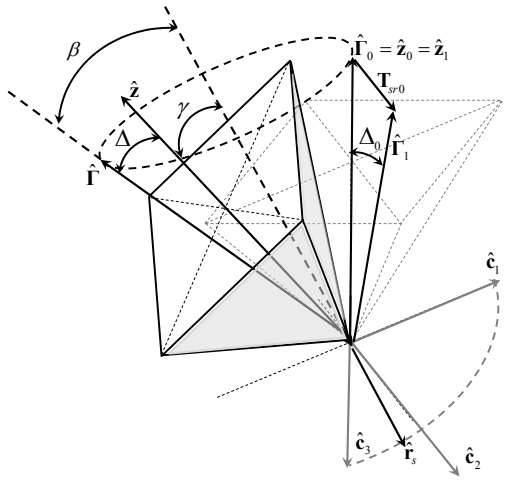

Fig. 17 Long term solar pointing mechanics

The qualitative behaviour described above is proved by numerical simulations. In Fig. 18 the nutation angle Δ, the angle of aperture of the cone designed by the angular momentum with respect to the sun direction (cone angle β), and the angle between the $\hat{\mathbf{z}}$ axis and the sun (pointing angle γ) are plotted for Sail 1. A drift of the $\hat{\mathbf{z}}$ axis with respect to the sun pointing direction begins when heliostability is absent (the cone angle and the pointing angles increase), but the main issue is represented by the impulsive behavior of the nutation angle, which increases rapidly when heliostability is recovered. However, the dissipative action of the dampers smoothens it before another eclipse occurs and overall stability is maintained.

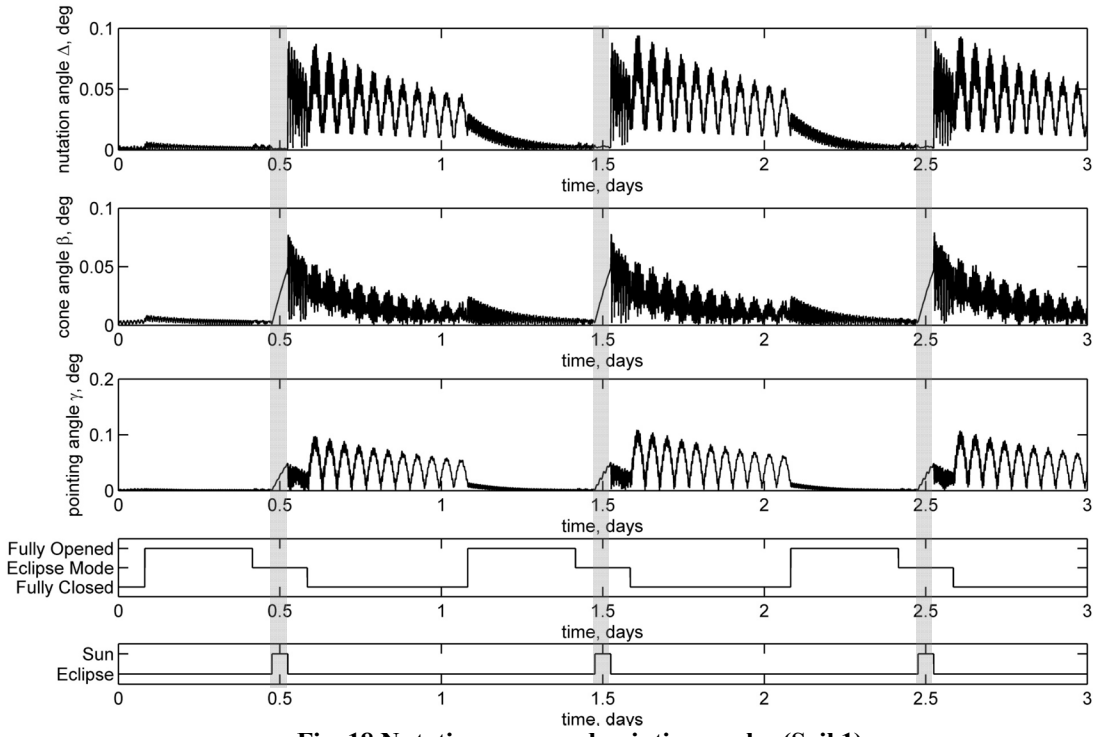

Fig. 18 Nutation, cone and pointing angles (Sail 1)

Year-long simulations are used to show the extended behaviour of the proposed concept. In Fig. 19 the attitude of Sail 1, Sail 2 and Sail 3 is represented by means of the pitch and yaw angles, while Fig. 20 shows the pointing angles for the same sails. It is known that eclipses are present only during specific seasons, and this is reflected in that deviations from the sun-pointing condition increase during these periods compared to other times. It is also noteworthy that the biggest deviation from the nominal working attitude occurs in the case of Sail 2, where some spikes reach an amplitude up to 2.5 deg, while for the other two sails the deviations remain confined in a fraction of degree.

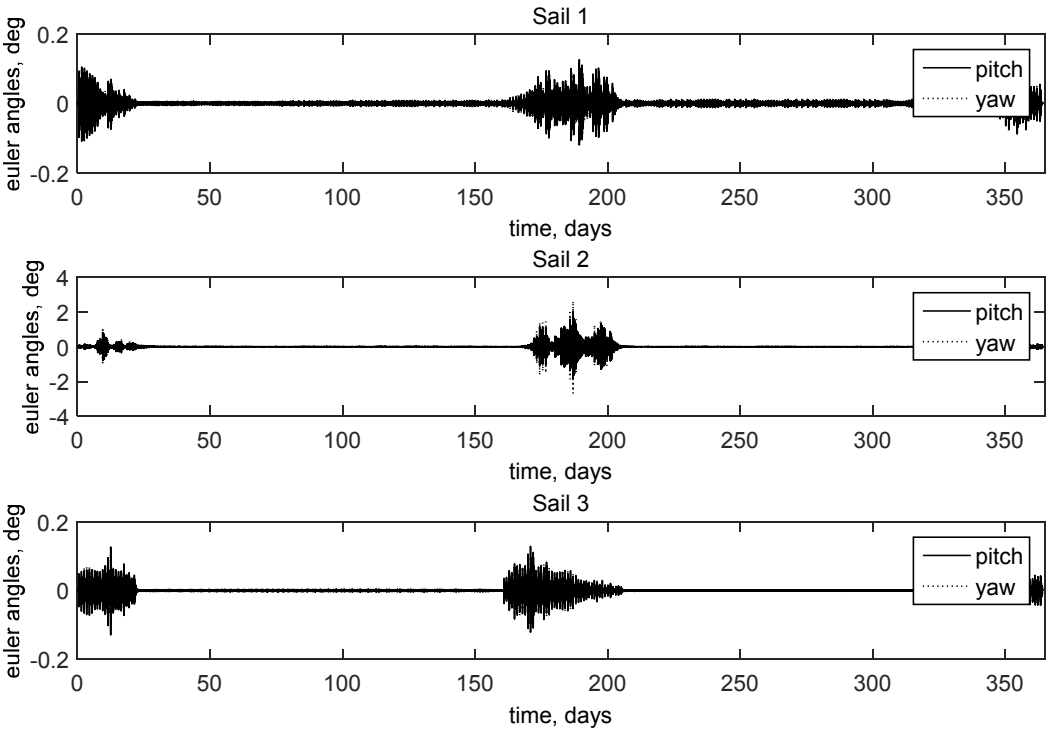

Fig. 19 Euler angles during one year for Sails 1, 2 and 3

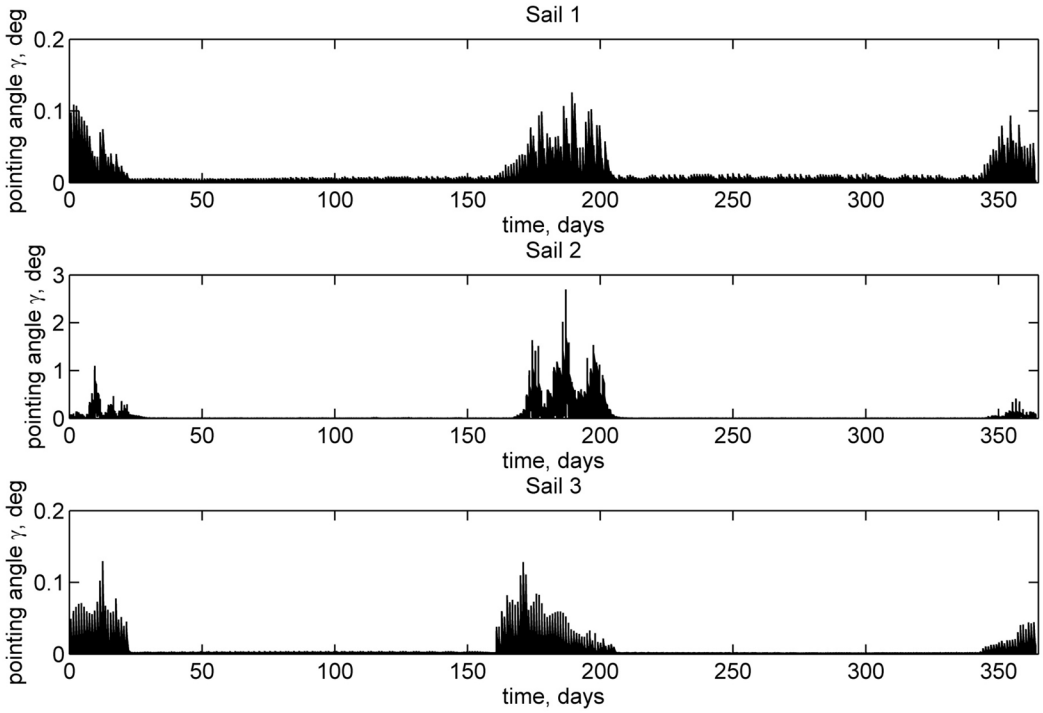

Fig. 20 Pointing angle during one year for Sails 1, 2 and 3

Finally, the performance in terms of orbit raising of the three configurations have been compared. Fig. 21 shows the increment of the semi-major axis during one year for the three stable sails, and Table 3 summarises the core performance indexes. Specifically, Sail 2 obtains the best performance exploiting both its greater area and the high value of the design factor b/l, as also shown in the numeric data summarized in Table 3. A significant increase in altitude is also obtained by Sail 1, but Sail 3, which has a $b/l = 1$ and a limited closure angle for stability reasons, cannot perform to a similar degree. The same table shows the averaged decrease of the spin rate over a year for the three sail configurations, and it is therefore suggested that a small heliogyro device may be required to regulate the spin rate over longer missions.

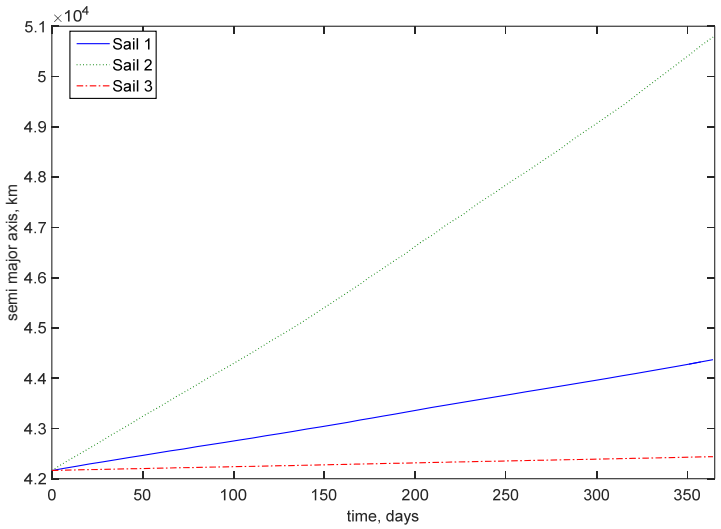

Fig. 21 Orbit semi major axis during one year, starting from GEO, for the three stable sails

Table 3 Sail performance over 1 year

Performance	Sail 1	Sail 2	Sail 3	Sail 4 *
Orbit raising rate, km/year	$+2.2\cdot10^{3}$	$+8.6\cdot10^{3}$	$+2.8\cdot10^{2}$	-
Maximum sun pointing deviation, deg	$1.3\cdot10^{-1}$	$2.7\cdot10^{0}$	$1.3\cdot10^{-1}$	$1.8\cdot10^{2}$
Spin decrease rate, rad/(s year)	$-2.8\cdot10^{-3}$	$-3.2\cdot10^{-3}$	$-6.5\cdot10^{-4}$	-
Minimum working orbit altitude, km	$1.7\cdot10^{4}$	$2.8\cdot10^{4}$	$5\cdot10^{3}$	-

* Unstable

Table 3 also summarizes the results of a parametric study performed to find the minimum operable orbit altitude for which the sail may operate despite the increase of the gravity gradient effects on the satellite motion. In fact, in decreasing the altitude of the orbit, both the fraction of orbit in eclipse and the gravity gradient torque magnitude

increase, which implies that the analytical results of Fig. 8 and Fig. 9 are no longer valid. Sail 2 provides the worst performance (highest minimum operable altitude) due to its large area and design ratio, while the best performance (lowest minimum operable altitude) is achieved by Sail 3, which exploits its reduced design ratio.

Conclusions

The concept of Quasi-Rhombic Pyramid (QRP) solar sail was explored in this paper. The QRP shape provides a passive, self-stabilizing effect around two axes under solar radiation pressure such that the apex of the pyramid passively points towards the Sun, with some support derived from spin about the third axis. Variation in the boom flare angles changes the effective area-to-mass ratio of the spacecraft and altitude adjustment may be achieved as a consequence.

Analytical, linearized techniques were used to define stability regions of the sail in the configuration space in the short period, and these results were verified for up to one year through numerical simulations. This work took into account full attitude and orbital dynamics, eclipses and gravity gradient torques, in addition to the boom configuration change and revealed that the concept can offer an increase of orbit altitude in the order of few thousand km per year, for a CubeSat-like bus with 1-meter booms in geostationary orbit. Lower increases are to be expected in lower orbits. It is worth underlining that this result is obtained without any expenditure of propellant or need of active attitude control: once the spacecraft is correctly spinning, the only actuation necessary is the opening/closing of the booms. It was also found that the concept becomes unfeasible below approximately 10,000 km a due to the extended duration of the eclipses combined with the magnitude of the gravity gradient torque. It is therefore envisaged that this concept can be used for mid- to high-altitude orbits, such as Geostationary Earth Orbits (GEO): examples are reaching higher orbits, i.e. from Medium Earth Orbit (MEO) to GEO or graveyarding of geostationary spacecraft, particularly when the propellant onboard has been depleted.

Acknowledgments

The author Leonard Felicetti would like to thank the School of Engineering of University of Glasgow for having hosted him as an Honorary Research Associate, giving him the opportunity to execute this project. Moreover, the same author would like to thank Prof. Giovanni B. Palmerini, who allowed this visiting period during the author's post-doctoral research in Sapienza - University of Rome.

References

[1] Tsu, T.C., "Interplanetary Travel by Solar Sail", *ARS Journal,* Vol. 29, pp. 422-427, 1959

[2] Heiligers, J., Ceriotti, M., McInnes, C.R., et al. "Displaced geostationary orbit design using hybrid sail propulsion", *Journal of Guidance, Control, and Dynamics,* Vol.34, No, 6, pp.1852-1866, doi: 10.2514/1.53807, 2011.

[3] Ceriotti, M., McInnes, C.R., "Generation of optimal trajectories for Earth hybrid pole-sitters", *Journal of Guidance, Control, and Dynamics,* Vol.34, No. 3, pp. 847-859, doi: 10.2514/1.50935, 2011.

[4] Mengali, G., Quarta, A.A. "Near-optimal solar-sail orbit-raising from low Earth orbit", *Journal of Spacecraft and Rockets*, Vol.42, No 5, pp. 954-958, doi: 10.2514/1.14184, 2005.

[5] Stolbunov, V., Ceriotti, M., Colombo, C., et al., "Optimal law for inclination change in an atmosphere through solar sailing", *Journal of Guidance, Control, and Dynamics,* Vol.36, No 5, pp.1310-1323, doi: 10.2514/1.59931, 2013.

[6] Macdonald, M., McInnes, C.R. "Analytical control laws for planet-centred solar sailing", *Journal of Guidance, Control, and Dynamics,* Vol. 28, No. 5, pp. 1038-1048, doi: 10.2514/1.11400, 2005.

[7] Wie, B., Murphy, D., "Solar-Sail Attitude Control Design for a Flight Validation Mission", *Journal of Spacecraft and Rockets,* Vol.44, No. 4, pp.809-821, doi: 10.2514/1.22996, 2007.

[8] Wie, B., "Solar sail attitude control and dynamics, part 1", *Journal of Guidance, Control, and Dynamics,* Vol. 27, No. 4, pp.526-535, doi: 10.2514/1.11134, 2004.

[9] Funase, R., Shirasawa, Y., Mimasu, Y., Mori, O. Tsuda, Y., Saiki, T., Kawaguchi, J., "On-orbit verification of fuel-free attitude control system for spinning solar sail utilizing solar radiation pressure", *Advances in Space Research*, Vol. 48, No. 11, pp. 1740-1746doi:10.1016/j.asr.2011.02.022, 2011

[10] Johnson, L., Whorton, M., Heaton, A., et al., "NanoSail-D: A solar sail demonstration mission", *Acta Astronautica*, Vol. 68, No. 5-6, pp. 571–575, doi: 10.1016/j.actaastro.2010.02.008, 2011.

[11] Shmuel, B., Hiemstra, J., Tarantini, V., et al., "The Canadian Advanced Nanospace eXperiment 7 (CanX-7) Demonstration Mission: De-Orbiting Nano- and Microspacecraft", *26th AIAA/USU Small satellite conference*, USA, 2012.

[12] Lappas, V., Adeli, N., Visagie, L., et al., "CubeSail: A low cost CubeSat based solar sail demonstration mission", *Advances in Space Research*, Vol.48, No.11, pp. 1890-1901, doi: 10.1016/j.asr.2011.05.033, 2011.

[13] Krivov, A.V., Sokolov, L.L., Dikarev, V.V., "Dynamics of Mars-orbiting dust: Effects of light pressure and planetary oblateness", *Celestial Mechanics and Dynamical Astronomy,* Vol.63, No. 3-4, pp.313-339, doi: 10.1007/bf00692293, 1995.

[14] Battin, R.H. An introduction to the mathematics and methods of astrodynamics. Revised edition ed. AIAA, New York, 1999.

[15] Borja, J.A., Tun, D., "Deorbit process using solar radiation force", *Journal of Spacecraft and Rockets,* Vol.43, No.3, pp.685-687, doi: 10.2514/1.9508, 2006.

[16] Gao, Y., "Near-optimal very low-thrust earth-orbit transfers and guidance schemes", *Journal of Guidance, Control, and Dynamics,* Vol.30, No.2, pp.529-539, doi: 10.2514/1.24836, 2007.

[17] Schaub, H., Junkins, J.L. Analytical Mechanics of Space Systems, 2nd Edition ed. AIAA, Reston, VA, USA 2009.

[18] Wu, S., Haug, E., "Geometric non-linear substructuring for dynamics of flexible mechanical systems", *International Journal for Numerical Methods in Engineering*, Vol. 26, pp.2211-2226, 1988.

[19] McInnes, C.R., "Artificial Lagrange points for a partially reflecting flat solar sail", *Journal of Guidance, Control, and Dynamics*, Vol. 22, No.1, pp. 185-187, doi: 10.2514/2.7627, 1999.

[20] Hughes,P.C., Spacecraft Attitude Dynamics, Dover Books on Aeronautical Engineering, 2005

[21] Molostov, A.A., Shvartsburg, A.A., "Heliocentric halos for a solar sail with absorption", *Soviet Physics Dokladv*, Vol.37, No.4, pp. 149–152, 1992.

[22] Nobari, N.A., Misra, A.K., "Attitude Dynamics and Control of Satellites With Fluid Ring Actuators", *Journal of Guidance, Control, and Dynamics*, Vol. 35, No. 6, pp. 1855-1864, 2012

[23] Ceriotti, M., Harkness, P., McRobb, M. "Variable-geometry solar sailing: the possibilities of the quasi-rhombic pyramid". In: Macdonald, Malcolm (ed.) *Advances in Solar Sailing*. Series: Springer Praxis Books: Astronautical Engineering . Springer in association with Praxis Publishing, pp. 899-919, 2014

[24] Harkness, P., McRobb, M., Lützkendorf, P., Milligan, R., Feeney, A., Clark, C., "Development status of AEOLDOS – A deorbit module for small satellites", *Advances in Space Research*, Vol. 54, No. 1, pp. 82-91, 2014.

[25] Wie. B., "Solar Sail Attitude Control and Dynamics, Part Two", *Journal of Guidance, Control, and Dynamics*, Vol. 27, No. 4, pp. 536-544, 2004

[26] Lawrence, D.A., Whorton. M. S., "Solar Sail Dynamics and Coning Control in Circular Orbits", *Journal of Guidance, Control, and Dynamics*, Vol. 32, No. 3, pp. 974-985, 2009.

[27] Fekete, T. A., Sackett, L. L., and von Flotow, A. H., "Trajectory Design for Solar Sailing from Low-Earth Orbit to the Moon," *Advances in the Astronautical Sciences*, Vol. 79, Feb. 1992, pp. 1083–1094.

[28] Macdonald, M., McInnes, C. R., "Analytical Control Laws for Planet-Centred Solar Sailing," *Journal of Guidance, Control, and Dynamics*, Vol. 28, No. 5, 2005, pp. 1038-1048, doi: 10.2514/1.11400.

[29] Macdonald, M., McInnes, C. R., "Realistic Earth Escape Strategies for Solar Sailing," *Journal of Guidance, Control, and Dynamics*, Vol. 28, No. 2, 2005, pp. 315-323, doi: 10.2514/1.5165.

[30] Coverstone, V. L., Prussing, J. E., "Technique for Escape from Geosynchronous Transfer Orbit Using a Solar Sail," *Journal of Guidance, Control, and Dynamics*, Vol. 26, No. 4, 2003, pp. 628-634, doi: 10.2514/2.5091.

[31] Borja, J. A., Tun, D., "Deorbit Process Using Solar Radiation Force," *Journal of Spacecraft and Rockets*, Vol. 43, No. 3, 2006, pp. 685-687, doi: 10.2514/1.9508.

[32] Mengali, G., Quarta, A. A., "Earth Escape by Ideal Sail and Solar-Photon Thrustor Spacecraft," *Journal of Guidance, Control, and Dynamics*, Vol. 27, No. 6, 2004, pp. 1105–1108.

[33] Fieseler, P. D., "A Method for Solar Sailing in a Low Earth Orbit," *Acta Astronautica*, Vol. 43, No. 9–10, 1998, pp. 531-541, doi: 10.1016/S0094-5765(98)00175-1.

[34] Mengali, G. and Quarta, A. A., "Near-Optimal Solar-Sail Orbit-Raising from Low Earth Orbit," *Journal of Spacecraft and Rockets*, Vol. 42, No. 5, 2005, pp. 954-958, doi: 10.2514/1.14184

[35] Morgan, T. O., "The Inclination Change for Solar Sails and Low Earth Orbit," *Advances in Astronautical Sciences*, Univelt, San Diego, CA, 1979, pp. 559–573.

[36] Stolbunov, V., Ceriotti, M., Colombo, C. and McInnes, C. R., "Optimal Law for Inclination Change in an Atmosphere through Solar Sailing," *Journal of Guidance, Control, and Dynamics*, Vol. 36, No. 5, 2013, pp. 1310-1323, doi: 10.2514/1.59931.

[37] Tsuda, Y., Mori, O., Funase, R., Sawada, H., Yamamoto, T., Saiki, T., Endo, T., Kawaguchi, J., Flight status of IKAROS deep space solar sail demonstrator, *Acta Astronautica*, Vol. 69, No. 9–10, Nov.–Dec. 2011, pp. 833-840, doi: 10.1016/j.actaastro.2011.06.005.